Journal of Magnetism and Magnetic Materials 115 (1992) 333–341
North-Holland

Investigation on Co–Cr micro-strips for VBLM *

J.G.Th. te Lintelo [a], J.C. Lodder [a], J. Engemann [b] and Th.J.A. Popma [a]

[a] *MESA Research Institute, University of Twente, P.O. Box 217, 7500 AE Enschede, The Netherlands*
[b] *University of Wuppertal, Fuhlrott Str. 10, W-5600 Wuppertal 1, Germany*

Received 12 November 1991; in revised form 21 May 1992

Hard magnetic strips can be used for bit stabilization in a VBLM. For this stabilization the magnetic strayfield of the strips induce potential wells for the bits. However, by dimensioning a material into strips the magnetic properties and therefore the potential wells change. In this paper the relation between magnetic properties and shape of Co–Cr micro-strips is investigated. Furthermore the influence of both magnetic properties and shape of the strips on the magnetic strayfield is simulated.

1. Introduction

For a successful operation of the Vertical Bloch Line Memory proposed in 1983 (VBLM) [1], a reliable propagation of the individual bits, i.e. Vertical Bloch Line (VBL) pairs and gaps, is of crucial importance. This propagation is studied by several authors resulting in general considerations on the material [2], and also in optimized stability and operation margins for drive- and in-plane fields [3,4]. However further research is needed on pinning sites in the garnet film that cause an unreliable scatter in the VBL coercivity [5,6]. Also exact knowledge of the bit stabilizing magnetic in-plane field is desirable because its form and amplitude define the physical bit locations. VBL's can be stabilized by an in-plane magnetic strayfield H_{ip} along stripe domains, according to

$$H_{ip}(x) = H_{ip0} \cos\left(\frac{x}{2\Lambda_0}\right), \qquad (1)$$

where Λ_0 is the Bloch line width parameter and H_{ip0} is of the order of 0.5 kA/m [2]. The x-direction is pointing along the domain wall of the garnet as is shown in fig. 1.

Bit stabilization can be achieved by different methods [7], however an overlay of hard magnetic strips is thought to be the most practical solution, because of power consumption and bit density reasons [8].

In fig. 1 a schematic view is given of the principle of VBL stabilization by magnetic strips. Magnetic strips are located on top of a garnet which exhibits the magnetic information (i.e. presence or absence of a VBL-pair) in domain walls of stabilized stripe domains. The strayfield of the overlay of strips will then induce a modulated pattern, according to eq. (1), along those domain walls. To obtain a stable device the strips must be hard magnetic. A spacer layer is put in between strips and garnet to exclude stress influ

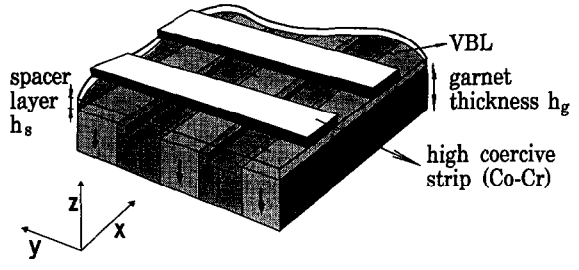

Fig. 1. Hard magnetic strips excerting a modulated strayfield along the stripe domain walls in a uniaxial garnet.

Correspondence to: Dr. J.C. Lodder, MESA Research Institute, University of Twente, P.O. Box 217, 7500 AE Enschede, The Netherlands.

* Presented at the International Conference on Magnetic Films and Surfaces, 26–30 August 1991, Glasgow, Scotland.

ences in the garnet and to obtain a smoother decrease of the strayfield amplitude along the z-direction of the domain wall.

In this paper we report on the magnetic properties of Co–Cr micro-strips that have, in contrast to other for this purpose investigated materials like Co–Pt [8] and Co–Ni [9], a perpendicular magnetic anisotropy. By dimensioning this Co–Cr into strips the magnetic properties change, in comparison to the as-sputtered samples, by means of a changing demagnetizing factor. This demagnetization is derived both experimentally and theoretically.

To investigate the consequences of perpendicular magnetization for the bit stabilizing in-plane field, a simulation program was developed that studies the strayfield as a function of the geometry of the overlay and as a function of the shape and size of the strips (tilted sideflanks and magnetization vector).

2. Experimental

2.1. Preparation

Co–Cr films were rf sputtered from different alloyed targets (Cr content: 19, 21 and 23 at%) under optimized conditions ($V_{rf} = -1.6$ kV, $P_{ar} =$ 0.4 Pa) in a Leybold Z400. The sample composition was measured by EDX.

Photolithography was performed using a positive resist (Shipley S1400-31), and followed by ion beam milling ($V_{acc} = 500$ V, $I_{cath} = 12.5$ mA, Ar flow = 200 sccm) which caused no annealing effects on the Co–Cr. The strip width was kept in the order of 5 μm and the period was varied (8, 10, 15 and 20 μm). Because of this changing period different exposure times were needed which resulted in a varying strip shape and width.

The shape was determined from SEM cross-sections, and as is shown in fig. 2 the strips demonstrate a tilting of the sideflanks of the strip. In table 1 the sideflank angles (α_L and α_R; see fig. 3 are listed, showing that angles smaller than 45° can technologically easily be obtained for these relatively thick films.

Relatively thick films and large stripwidths were used for this investigation, in comparison to the strip thicknesses and widths used for VBL stabilization [8,9]. This is due to the fact that the sensitivity of the magnetic measurements require a minimum magnetic volume and thus relatively large and thick specimens. The size of the specimens (1×1 cm^2) also prevented the use of e-beam lithography. The strip thickness and widths are a compromise of these factors, and determined by our main interest of investigating de-

Table 1
Geometrical-, compositional- and magnetic information on the investigated samples

Sample no.	Thickness [nm]	Cr content [at%]	M_s [kA/m]	K_1 [kJ/m^3]	W_{bottom} [μm]	α_L & α_R [°]	Period [μm]	N_z (theor.)	N_x (exp.)	N_z (exp.)
080191	825	18.6	474	118	5.00	40	10	0.840	0.132	0.684
250291	910	19.2	447	113	4.20	34	10	0.790	0.186	0.721
260291	870	18.1	440	104	4.80	29	10	0.821	0.130	0.741
060391	910	19.5	485	157	5.84	34	10	0.870	0.052	0.907
070391	900	23.0	299	70	5.12	33	10	0.827	0.097	0.801
080391-1	700	19.1	463	145	4.00	36	15	0.814	0.125	0.955
080391-2	700	18.9	469	148	4.25	42	15	0.814	0.157	0.836
080391-3	700	19.0	464	150	4.75	47	20	0.837	0.106	0.864
080391-4	700	19.2	457	135	4.00	42	10	0.820	0.088	0.869
080391-5	700	18.4	451	123	5.30	34	8	0.880	0.071	0.794
080391-6	700	18.8	469	141	4.50	47	8	0.846	0.042	0.922
280591A-1	843	18.2	567	198	5.50	31	20	0.832	0.048	0.956
280591A-2	843	18.6	567	190	4.70	37	15	0.811	0.106	0.807
280591A-4	843	18.1	567	182	4.50	24	15	0.806	0.056	0.940

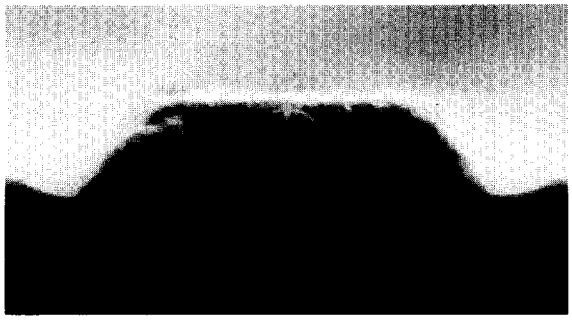

Fig. 2. SEM photograph of a cross-section of one strip (sample 080391).

magnetizing effects. The demagnetizing effects depend on the strip thickness to strip width ratio and has thus to be rather large. However, this will contribute to a general understanding of bit stabilization by hard magnetic strips when strips are scaled down in size.

2.2. Magnetic measurements

The investigated magnetic strips have a uniaxial anisotropy perpendicular to the substrate (z-direction; K_1, K_2) and an induced shape anisotropy lying in the plane of the film (see fig. 3). For the present it is assumed that the applied magnetic field is high enough to keep the magnetization parallel to the field direction, and to establish the single domain state. The torque per unit volume then becomes:

$$L = -\left(K_1 + K_2 - \tfrac{1}{2}\mu_0 M_s^2 (N_\perp - N_\parallel)\right) \sin 2\phi + \tfrac{1}{2}K_2 \sin 4\phi, \quad (2)$$

where $N_\perp$ and $N_\parallel$ denote the geometrical demagnetization factor perpendicular and in-plane of the measurement plane, respectively [10].

Performing torque measurements with the applied field rotating in three different planes [11] (i.e. PM, LM and TM; see fig. 3), N_x and N_z can then be obtained (assumption $N_y = 0$). N_x is derived from PM measurement, N_z from LM or TM measurement. Because the torque equations for the LM and TM mode are coupled, K_1 has been determined from the as-sputtered sample. This introduces an error in N_z because in the anisotropy constant derivation also magnetostriction is included [10], which will be affected by the ion milling.

3. Experimental results

In fig. 4 an example is shown of torque curves of strips, for the three different modes, together with the torque curve of the corresponding as-sputtered sample. As can be seen from the PM measurement, a strong induced shape anisotropy is present in the xy-plane. This shape anisotropy causes the LM and TM measurements to differ

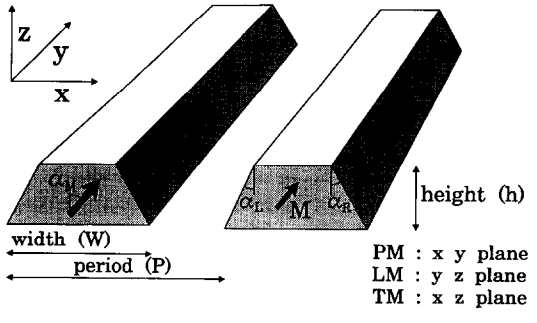

Fig. 3. Geometry of the strips and definition of the in this paper used parameter notations.

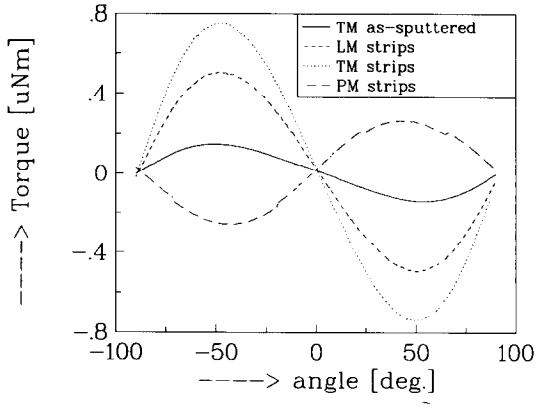

Fig. 4. Comparison between torque curves of the as-sputtered sample and corresponding strips (080391-2).

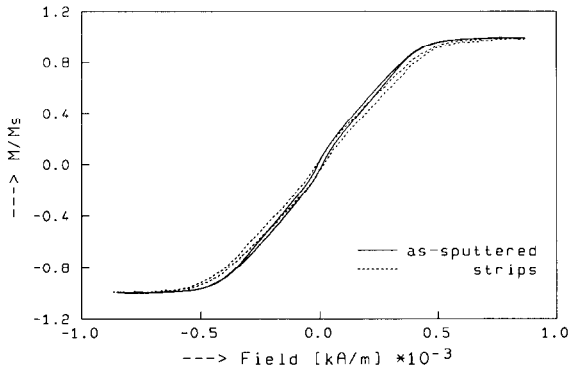

Fig. 5. In-plane hysteresis curves for strips 080391-2 (dashed line), compared to the as-sputtered sample 080391-2 (solid line).

by a factor N_x (see eq. (2)). The demagnetization factors derived from torque measurements are given in table 1.

In figs. 5 and 6 typical hysteresis curves are shown. In fig. 5 the in-plane hysteresis curve of the as-sputtered sample (solid line) and the strips (dashed line) are compared, showing a higher anisotropy field for the latter. Whereas the magnetic field was applied in the x-direction (see fig. 3), this can be attributed to the extra demagnetization in x-direction, which could also be seen in the torque measurements. In fig. 6 the perpendicular hysteresis curves of an as-sputtered sample (solid line) and strips (dashed line) are shown. Both curves show a typical shoulder, and shearing of the curve due to demagnetization. In fig. 7 the

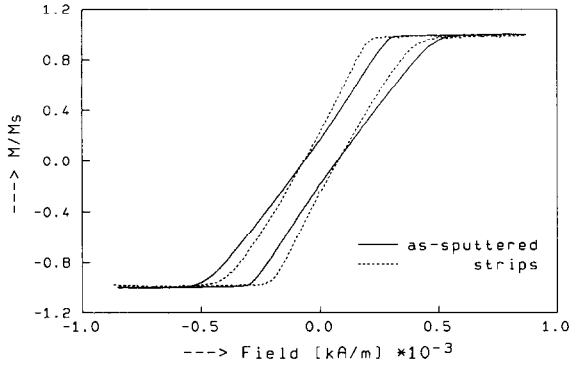

Fig. 6. Perpendicular hysteresis curves for strips 080391-2 (dashed line), compared to the as-sputtered sample 080391-2 (solid line).

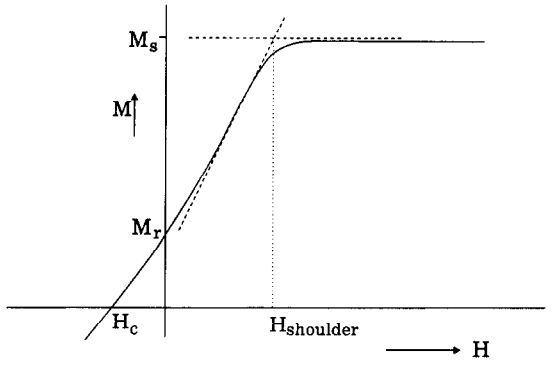

Fig. 7. Definition of the estimated 'shoulder field'.

'shoulder field' is defined, as the intersection of the line which shears the upper part of the hysteresis curve and the saturation magnetization. This shearing in the upper part is performed at 80% of M_S, because in this point the decrease in magnetization with applied field is largest (for these investigated films). Theoretically the shearing and the 'shoulder field' depend on the demagnetization field H_D

$$H_D = N_z M, \tag{3}$$

where M is the magnetization.

A smaller demagnetization of the sample with the strips thus results in less shearing and a smaller 'shoulder field'.

In fig. 8 the difference in 'shoulder field', divided by the saturation magnetization, of the as-sputtered sample and the strips is depicted as a function of the demagnetization factor. Here the N_x factor is used because no perpendicular anisotropy is involved in its calculation, so reducing the error in comparison with N_z. It can be seen that the samples show a relatively small scatter around the line of the overall demagnetization factor, showing the theoretical dependence: $\Delta H_{\text{shoulder}} = (1 - N_z)M_s$.

The above mentioned behaviour causes the remanence and coercivity to increase. In order to quantify the relation with the demagnetization factor we derived a strongly simplified relation:

$$\left(\frac{(H_{c1}/H_{c2})M_{r2} - M_{r1}}{M_{r1}} \right) = \frac{N_x}{N_z}, \tag{4}$$

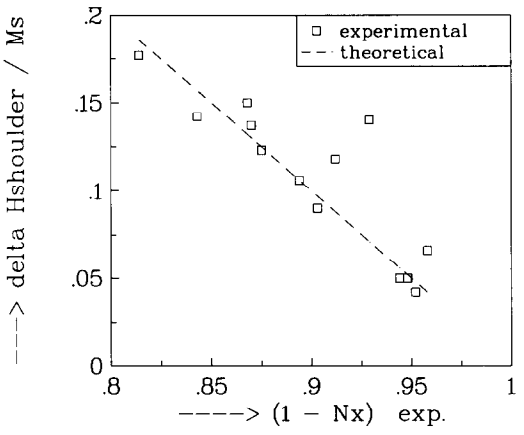

Fig. 8. The difference in 'shoulder field' of the as-sputtered sample and strips divided by the saturation magnetization, as a function of the demagnetization factor.

where the index 1 denotes the as-sputtered sample and the index 2 the into strips dimensioned sample. The first term in eq. (4), which determines a normalized increase in remanence related to the coercivity, will be called the 'remanence parameter'.

In fig. 9 the experimental remanence parameter is shown together with a theoretical line which indicates the value of N_x divided by N_z. As can be seen from this figure the experimental curve shows principal agreement with the theoretical curve, however the value of the experimental

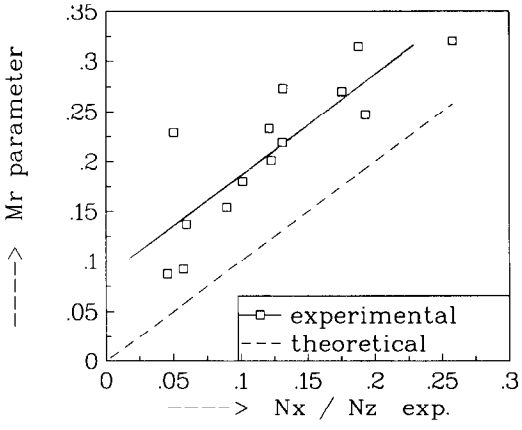

Fig. 9. Remanence parameter (eq. (4)) as a function of the demagnetization ratio N_x/N_z.

curve is too large (or the demagnetization ratio is too small). This will be further discussed in section 4.

Figs. 8 and 9 indicate that the increase in remanence can be correlated to an experimental obtained demagnetization factor. However the increase in remanence depends on the history of the sample which is a complex system where the dependence on the demagnetization factor of 'shoulder field', initial slope and coercive force play and interacting role. Besides this it should be noted that the demagnetization factor is an averaged factor, whereas magnetic properties will depend on their local 'magnetic' environment.

4. Demagnetization factor calculation for strips

From the above can be concluded that by dimensioning the shape of ferromagnets the demagnetization factor will change, and therefore its magnetic properties will change. Especially the increase in remanence is important because remanence determines the amplitude of the modulated strayfield of eq. (1). The relation between shape and demagnetization factor should thus be incorporated in designing an overlay of strips for VBL stabilization.

The demagnetization factor can be calculated for a uniformly magnetized rectangular bar by direct integration over the pole densities on top and bottom planes (see the Appendix). In an assembly of strips however the strayfields of all the strips will interact, and therefore an additional demagnetizing factor is introduced.

In fig. 10 the result of the overall demagnetization factor is shown as a function of the strip period. As can be seen from this figure, the demagnetization factor is equal to one if the period equals the strip width (i.e. infinite plate) and then it slowly decreases, with increasing period, to the demagnetization factor of one strip which has no magnetostatic interactions.

Because the strips exhibit tilting of the sideflanks (see fig. 2), we also calculated this tilting influence on the demagnetization factor. For this a stray field simulation program is used (see also section 5) which sums the strayfield H_z inside a

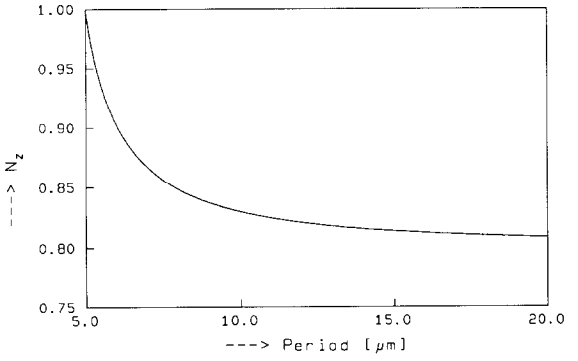

Fig. 10. Demagnetization factor N_z of an assembly of strips as a function of the period. Strip parameters: $w = 5$ μm, $h = 1$ μm.

strip over a grid of 7000 points in the xz plane (see fig. 3). By dividing the mean value of H_z by M_s, the volume averaged demagnetization factor can be obtained for an assembly of strips.

In fig. 11 an example is given of the demagnetization factor of an assembly of strips as derived theoretically (see the appendix), and by the simulation program for tilting sideflank angle $\alpha_L = \alpha_R = 0°$ and $\alpha_L = \alpha_R = 30°$ (see fig. 3). As can be seen, the simulated demagnetization factor coincides for a rectangular strip with theory. Also can be concluded that a tilting of the sideflanks has a strong influence on the demagnetization factor.

In fig. 12 the theoretical demagnetization factor, including tilted sideflanks and the demagnetizing influence of the other strips, is compared to the experimental factors as derived in section 3. The experimentally determined factors show a large scatter with theory. This will be partly due to errors in determining the shape of the strips (the errors in thickness and width are in the order of 5%). Also the in the model assumed uniform magnetization is probably not attained because the torque coefficients show a large non-linear field dependence, and we know from other research that there is a chemical inhomogeneity in sputtered Co–Cr films [12,13].

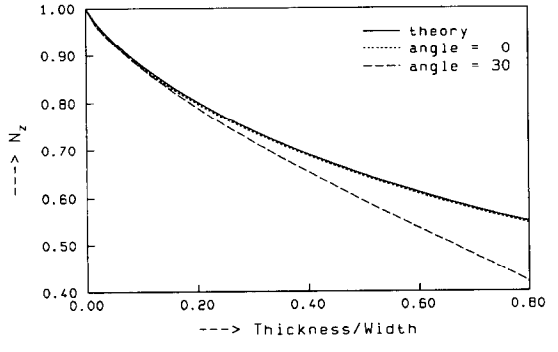

Fig. 11. Demagnetization factor of one strip, as derived from theory (solid line) and by simulation (dashed and dotted curves). The angle indicated in the legend denotes the tilting of the sideflanks of the strips (α_L and α_R). Strip parameters: $W = 3$ μm, $P = 6$ μm, h is varied.

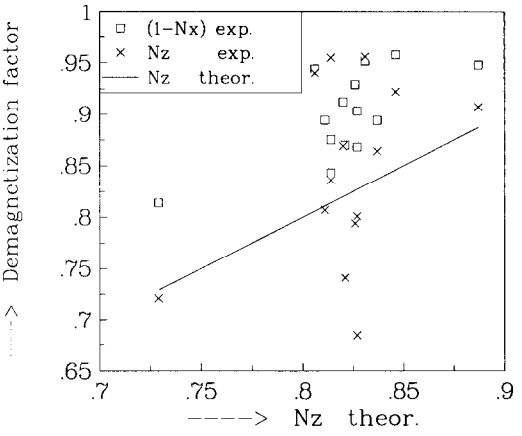

Fig. 12. Experimentally derived demagnetization factors N_x and N_z of an assembly of strips as a function of the theoretical demagnetization factor N_z.

From fig. 12 two things can be suggested. Firstly the experimentally obtained $(1 - N_x)$ appears to be in relatively good accordance to the theoretical N_z, however the mean value of N_x is too small. This could be attributed to a systematical error in demagnetization determination and could also explain why in fig. 8 the ratio of the demagnetization factor in x and z direction was too small. Secondly the experimentally derived N_z factor shows a larger scattering than N_x, and is in general smaller than $(1 - N_x)$. The scatter could be due to errors in K_1, caused by a probable altered magnetostriction. The difference in the experimental obtained N_z and $(1 - N_x)$, could indicate a non-zero N_y.

This leads to an overall conclusion that magnetic parameters are affected by their shape which can be correlated to the experimental demagneti-

zation factor in the x-direction. The theoretical calculation of the demagnetization factor as shown in figs. 10 and 11 must be regarded as a qualitative result showing the influence of shape and size of the strips on the demagnetization factor. For a more quantative comparison it appears that more parameters have to been included in the model.

5. Magnetic stray field simulation for strips

In the foregoing sections a relation between shape of the strips and magnetic properties was investigated. In this last section the influence of both shape and magnetic properties on the bit stabilizing strayfield is investigated by means of a simulation.

The simulation is based on calculating the field of a sheet with uniform pole density. As could be seen from the SEM cross-section in fig. 2, the investigated strips have their sideflanks under a certain angle. With the assumption of uniform magnetization in the strips this leads to a magnetic pole density on top surface of $M = +M_s \cos(\alpha_M)$ and bottom surface $M = -M_s \cos(\alpha_M)$. The left sideflank has an effective magnetization of $M = M_s \sin(\alpha_L - \alpha_M)$, whereas the right sideflank has $M = M_s \sin(\alpha_R + \alpha_M)$.

In this simulation the left and right sideflank angles (α_L and α_R, respectively), and also the magnetization vector angle (α_M, in the xz-plane), can be varied independently (see fig. 3). The strayfield is always calculated along the x-direction underneath the overlay of strips.

In the simulation use is made of saturated strips. Because an overlay of Co–Cr strips is not saturated but in remanence, we included a 'checkerboard' domain structure in the simulated strips. Taking the thickness depended domain period following the $\frac{1}{2}$-power law [14], and strip widths larger than 1 μm, no influence on the form of the stray field was observed for distances underneath the overlay larger than 1 μm (which is about 5 to 10 times the stripe domain period). Only the amplitude was lowered by the factor M_r/M_s. Thus for spacer layer thicknesses larger than 1 μm it is allowed to use the value of the remanence as M_s-value in the simulation of Co–Cr strips.

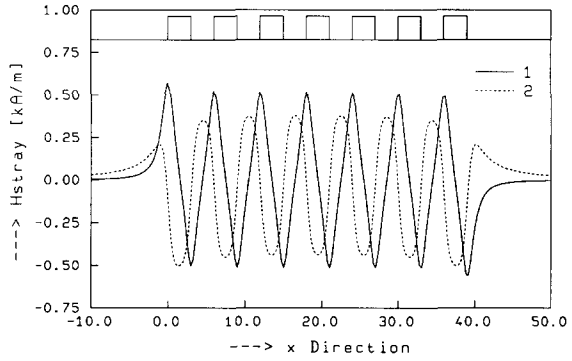

Fig. 13. The in-plane magnetic strayfield $H_x(x)$ of an overlay of strips. Strip parameters: $P = 6$ μm, $W = 3$ μm, $h = 50$ nm, $h_s = 1$ μm, $M = 80$ kA/m. Curve 1: $\alpha_M = 0°$ (perp.); curve 2: $\alpha_M = 90°$ (in-plane).

In fig. 13 an example is shown of the magnetic in-plane stray field of an overlay containing a few strips, which are magnetized in the perpendicular and in-plane direction. Comparing these two directions it can be seen that the stable VBL positions ($H_{ip} = 0$) are shifted.

From fig. 13 can also be seen that the first field maxima will cause a nonuniformity because its amplitude is larger than the inner field maxima. This effect can be visualized as strayfields superpositioned by the strayfield of a rectangular bar that has the width of the overlay of strips (see fig. 14). This causes the magnetic stray field of

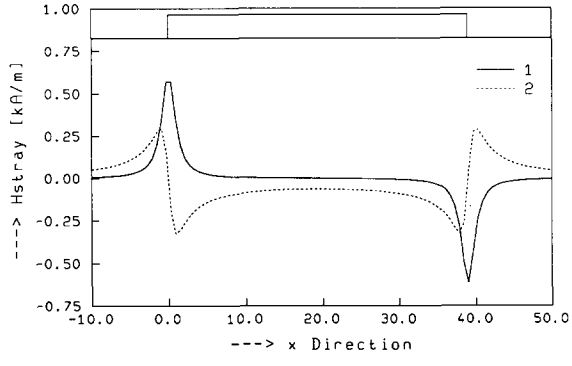

Fig. 14. The in-plane magnetic strayfield $H_x(x)$ of a rectangular bar with a width which equals the overlay as shown in fig. 13. Curve 1: $\alpha_M = 0°$ (perp.); curve 2: $\alpha_M = 90°$ (in-plane).

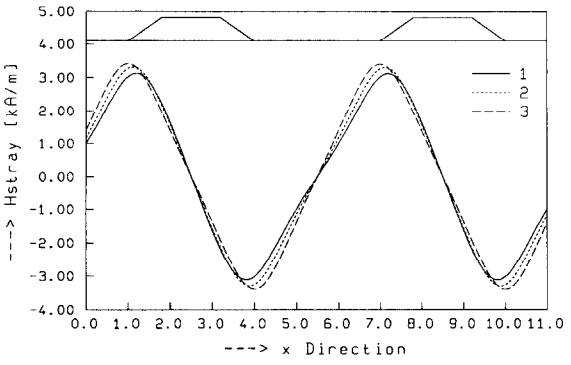

Fig. 15. The in-plane magnetic strayfield $H_x(x)$ of an overlay of magnetic strips with strip parameters: $P = 6$ μm, $W = 3$ μm, $h = 800$ nm, $h_s = 1$ μm, $M = 50$ kA/m). Curve 1: $\alpha_l = \alpha_r = 45°$; 2: $\alpha_l = \alpha_r = 30°$; 3: $\alpha_l = \alpha_r = 0°$.

the perpendicular magnetized strips to be symmetrical around the line of zero amplitude, whereas the in-plane magnetized strips have a shifted in-plane magnetic stray field. This shift causes an extra nonuniformity for the in-plane magnetized strips. For decreasing strip thicknesses (h) and increasing spacer layer thicknesses (h_s) these distorting effects will decrease.

Investigating the influences of the sideflanks we found that sideflanks angles smaller than 45° (which is technologically easily obtained) hardly have any influence for strip thicknesses below 1/10 of the strip width. This result holds for both the magnetization lying in-plane or perpendicular. In fig. 15 an example is shown for a relatively thick film.

From the simulation program can be concluded that optimum strip thicknesses have to be designed in correlation with garnet- and spacer thicknesses, as well strip width, period and remanence. For garnets and strip widths, which are mentioned in literature, a Co–Cr strip thickness of 50 nm and a remanent magnetization of 80 kA/m, is a good figure.

6. Conclusions

By dimensioning Co–Cr into micro-strips the magnetic properties change by means of a changing demagnetization factor. This demagnetization factor can be derived from experiment and shows a principal correlation with the change in magnetic parameters. Its influence on the increase of remanence of strips, in comparison with as-sputtered samples, is still under consideration. However this effect is of importance for designing an overlay of strips for VBL stabilization, because the remanence determines the amplitude of the bit stabilizing stray field.

From torque and VSM measurements followed that by dimensioning Co–Cr into strips, the effective anisotropy and coercivity increases. Perpendicular magnetized strips will therefore become more stable, in contrast to in-plane magnetic media, when going to smaller strip widths.

From simulation followed that perpendicular magnetic media can also be advantageous to in-plane magnetized media because of less nonuniformities, and that tilting of the sideflanks of the strips hardly has any influence on the shape of the stray field. This tilting however has a strong influence on the demagnetization factor.

Acknowledgements

The authors like to thank Dr. V. Kambersky from the Institute of Physics in Prague for valuable discussions. We also thank Mr. A.M. Otter for the SEM observations. This research has been financially supported by CAMST, a program of the EC.

Appendix. Demagnetization factor calculation for strips

The demagnetization factor of a uniformly magnetized rectangular bar can be obtained by integration over the pole densities on top and bottom faces, and is given by:

$$N_z = \frac{1}{\pi}\left(2\tan^{-1}\left(\frac{1}{q}\right) - \frac{1-q^2}{2q}\log(1+q^2) + q\log(q)\right), \qquad (A.1)$$

where q is defined as: $q = h/W$.

In an assembly of strips however the strayfields of all the strips will interact, and therefore an additional demagnetizing factor is introduced. The demagnetizing influence of the first strip on the second strip can be derived by integrating the magnetic strayfield of the first strip along the second strip:

$$N_{z,1\to 2} = \frac{1}{M}\left(\frac{1}{W}\int_P^{P+W} H_{z1}\,\mathrm{d}x\right)$$
$$= \frac{1}{W}\int_P^{P+W} \frac{-1}{\pi}\left(2\tan^{-1}\left(\frac{1}{q}\right) - \frac{1-q^2}{2q} \times \log(1+q^2) + q\,\log(q)\right)\mathrm{d}x. \quad \text{(A.2)}$$

By repeating this procedure for the third till Nth strip and taking reprocity of the fields into consideration, we find that the demagnetization factor of an overlay of strips is given by:

$$N_z = \frac{1}{N\pi}\sum_{j=0}^{N}\sum_{i=1-j}^{N-j} (iP-W)\tan^{-1}\frac{(iP-W)}{h} + (iP+W)\tan^{-1}\frac{(iP+W)}{h} - 2iP\tan^{-1}\frac{iP}{h} + \frac{(iP-W)^2}{4h} \times \log\left(1+\frac{h^2}{(iP-W^2)}\right) + \frac{(iP+W)^2}{4h} \times \log\left(1+\frac{h^2}{(iP+W^2)}\right) - \frac{i^2P^2}{2h}\log\left(1+\frac{h^2}{P^2}\right) - \frac{h}{4}\log\left(1+\frac{(iP-W)^2}{h^2}\right) - \frac{h}{4}\log\left(1+\frac{(iP+W)^2}{h^2}\right) + \frac{h}{2}\log\left(1+\frac{P^2}{h^2}\right).$$

Because the demagnetizing influence of a strip decreases very fast with distance, this equation can be approximated within 1% for $N > 8$ by

$$N_z = \frac{A_i}{W\pi}\sum_{i=0}^{\frac{N}{2}} (iP-W)\tan^{-1}\frac{(iP-W)}{h} + (iP+W)\tan^{-1}\frac{(iP+W)}{h} - 2iP\tan^{-1}\frac{iP}{h} + \frac{(iP-W)^2}{4h}\log\left(1+\frac{h^2}{(iP-W^2)}\right) + \frac{(iP+W)^2}{4h}\log\left(1+\frac{h^2}{(iP+W^2)}\right) - \frac{i^2P^2}{2h}\tan\left(1+\frac{h^2}{P^2}\right) - \frac{h}{4}\log\left(1+\frac{(iP-W)^2}{h^2}\right) - \frac{h}{4}\log\left(1+\frac{(iP+W)^2}{h^2}\right) + \frac{h}{2}\log\left(1+\frac{P^2}{h^2}\right),$$

with $A_i = 1$ for $i = 0$, $A_i = 2$ for $i > 0$.

References

[1] S. Konishi, IEEE Trans. Magn. MAG-19 (1983) 1838.
[2] G. Ronan, W. Glegg and S. Konishi, J. de Phys. 46 (1985) C6-127.
[3] J. Theile, R. Kosinski and J. Engemann, J. Magn. Magn. Mater. 62 (1986) 139.
[4] R. Kosinski, J. Magn. Magn. Mater. 83 (1990) 101.
[5] Y. Fedyunin, F. Friedlaender and J. Nyenhuis, IEEE Trans. Magn. MAG-26 (1990) 2523.
[6] H. Krause, J. Theile, R. Dahlbeck and J. Engemann, J. Magn. Magn. Mater. 95 (1991) 95.
[7] T. Suzuki, H. Asada, K. Matsuyama, E. Fujita, Y. Saegusa, K. Morikawa, K. Fujimoto, M. Shigenobu, K. Nakashi, H. Takamatsu, Y. Hidaka and S. Konishi, IEEE Trans. Magn. MAG-22 (1986) 784.
[8] Y. Maruyama, T. Ikeda, K. Fujimoto and R. Suzuki, IEEE Trans. Magn. MAG-24 (1988) 3027.
[9] J. Heidmann, R. Dahlbeck, H. Krause and J. Engemann, IEEE Trans. Magn. MAG-24 (1988) 3048.
[10] J. Worst, J.C. Lodder and T. Wielenga, Thin Solid Films 101 (1983) 75.
[11] S. Swaving, G.J. Gerritsma, J.C. Lodder and Th.J.A. Popma, J. Magn. Magn. Mater. 67 (1987) 155.
[12] T. Masuda, W.J.M.A. Geerts and J.C. Lodder, J. Magn. Magn. Mater. 95 (1991) 123.
[13] Y. Maeda and M. Takahashi, IEEE Trans. Magn. MAG-24 (1988) 3012.
[14] J. Kaczer, J. Simsova, R. Gemperle, L. Murtinova and J.C. Lodder, J. de Phys. 49 (1988) C8-1993.